



CHORUS

This is the accepted manuscript made available via CHORUS. The article has been published as:

Two-Step Phase Transition in SnSe and the Origins of its High Power Factor from First Principles

Antoine Dewandre, Olle Hellman, Sandip Bhattacharya, Aldo H. Romero, Georg K. H. Madsen, and Matthieu J. Verstraete

Phys. Rev. Lett. **117**, 276601 — Published 30 December 2016

DOI: [10.1103/PhysRevLett.117.276601](https://doi.org/10.1103/PhysRevLett.117.276601)

Two step phase transition in SnSe and the origins of its high powerfactor from first principles

Antoine Dewandre,^{1,2} Olle Hellman,^{3,4} Sandip Bhattacharya,⁵ Aldo H. Romero,^{6,7} Georg K. H. Madsen,⁸ and Matthieu J. Verstraete^{1,2}

¹*Department of Physics, Université de Liège, allée du 6 août, 17, B-4000 Liège, Belgium.*

²*European Theoretical Spectroscopy Facility www.etsf.eu*

³*Division of Engineering and Applied Science, California Institute of Technology, Pasadena, California 91125.*

⁴*Department of Physics, Chemistry and Biology (IFM),*

Linköping University, SE-581 83, Linköping, Sweden

⁵*ICAMS, Ruhr-Universität Bochum, 44780 Bochum, Germany*

⁶*Department of Physics, West Virginia University, 207 White Hall, 26506, WV, USA.*

⁷*Facultad de Ingeniera, Benemrita Universidad Autnoma de Puebla, 72570, Puebla, Pue., Mexico*

⁸*Institute of Materials Chemistry, TU Wien, A-1060 Vienna, Austria*

(Dated: October 19, 2016)

The interest in improving the thermoelectric response of bulk materials has received a boost after it has been recognized that layered materials, in particular SnSe shows a very large thermoelectric figure of merit. This result has received a large attention while it is now possible to conceive other similar materials or experimental methods to improve this value. Before we can now think in engineering this material it is important we understand the basic mechanism that explains this unusual behavior, where very low thermal conductivity and high thermopower result form a delicate balance between crystal and electronic structure. In this paper, we present a complete temperature evolution of the Seebeck coefficient as the material undergoes a soft crystal transformation and its consequences on other properties within SnSe by means of first principles calculations. Our results are able to explain the full range of considered experimental temperatures.

Thermoelectric (TE) materials and the thermoelectric effect are an interesting alternative energy source, harvesting waste heat from power production and other thermal engines. Despite their vast potential impact, only few materials are used in practice: most thermoelectric materials are highly toxic, expensive, and devices present too low efficiencies to compete with other forms of power generation in industry. The main concern in this field is to discover or design thermoelectric materials which deal with these issues. The efficiency of a TE material is quantified by the thermoelectric figure of merit $zT = S^2\sigma T/(\kappa_{el} + \kappa_l)$, which is the ratio of the electrical conductivity (σ), multiplied by the Seebeck coefficient (S) squared and the absolute temperature (T), over the thermal conductivity, which has both ionic (κ_l) and electronic (κ_{el}) contributions. The recent demonstration of $zT = 2.6$ in monocrystalline tin selenide[1] or $zT = 1.34$ in device form [2] has given a new breath to the field of thermoelectrics. By more than doubling the efficiency record for intrinsic bulk systems, SnSe has shown that economically competitive, non-toxic TE devices are within reach. The microscopic mechanism responsible for the performance is however not fully established, in particular due to sublimation effects in the high-T phase.

Bulk SnSe is a narrow band gap semiconductor which undergoes a phase transition spanning the temperature range from 600 K to 807 K, from a Pnma low-temperature phase illustrated in Fig. 1 (space group 62) to a Cmcm high-temperature phase (space group 63) [3]. Both are distorted phases of rock-salt Fm3m (the isolectronic structure of PbTe and SnTe). Exceptional values

of zT are obtained for two main reasons: the intrinsically low thermal conductivity (in both phases) and the strong enhancement of the carrier concentration and conductivity in the Cmcm phase. This intricate interplay opens perspectives for many other layered or heterostructure materials, and calls for a profound understanding of the mechanisms. Properties can then be further engineered, e.g. by doping [2, 4–6], nanostructuring [7–9] or strain [10, 11]. Therefore, it is expected that any results we obtain from the physical comprehension of SnSe can be extrapolated to many other layered materials as SnTe and SnS (as in Ref. [12]). While many authors have described the different physical properties of this material, there is still an incomplete picture of the thermoelectric response of SnSe over the whole temperature range.

In this paper, we offer a clear description of the experimental thermoelectric response of SnSe as a function of temperature. We perform advanced first principles calculations to elucidate the origin of the increase in carrier concentration and the nature of the phase transition. Carrier concentrations are determined from intrinsic defect energies in the low and high T phases. We find that the calculated carrier concentration is dominated by Sn vacancies. Defect thermochemistry results, and carrier concentrations, show a strong dependence on both structure and temperature. We calculate Seebeck coefficients including the temperature dependence of the chemical potential, Fermi distribution, and the structure. Our results are in excellent agreement with experiments. We clarify the complex phase transition pathway between Pnma and Cmcm, and show that the high-T Cmcm phase

is stabilized only when anharmonicity is included. Using harmonic phonon calculations and metadynamics simulations, we identify the sequence of elastic and phononic distortions which was suggested over 30 years ago by von Schnering and Wiedemeier [3]. The carrier concentrations are derived from intrinsic defect calculations within density functional theory. Perturbation theory is used for the harmonic phonon analysis[13], and the Temperature Dependent Effective Potential method[14], based on ab initio molecular dynamics, to calculate fully renormalized anharmonic effects and the complete P-T phase diagram. Metadynamics [15, 16] allows us to explore the Born-Oppenheimer surface to refine our understanding of the phase transition. Seebeck coefficients are calculated from the Boltzmann Transport Equation within the constant Relaxation Time Approximation[17]. Further details of the theoretical methods are given in S.I.

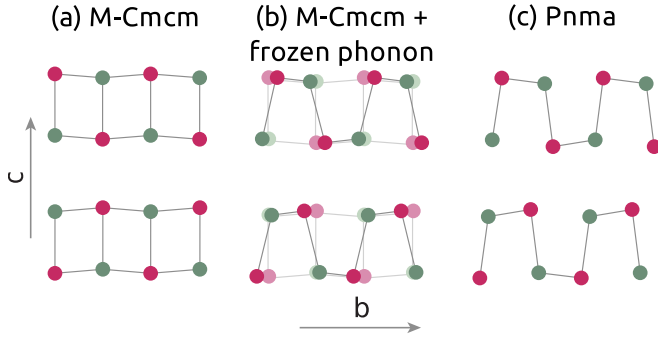


FIG. 1. Ball and stick model for both orthorhombic phases of SnSe. (a) Modified high-T Cmcm phase; (b) distortion of the modified Cmcm structure by the unstable phonon mode at Y which leads to the stable Pnma phase; (c) low-T Pnma phase.

We perform defect thermochemistry calculations to calculate defect formation energies, E_d , in the experimentally relevant Se rich limit. The results are shown in Fig. 2 versus the electron chemical potential μ_e for two experimental unit cells obtained at 790 K (Pnma) and 829 K (Cmcm)[18] and where atomic positions are relaxed. The dominant defect in both phases is the Sn vacancy ($\text{Vac}_{\text{Sn}}^{(2-)}$), which produces holes. The most striking difference between the two phases is that $\text{Vac}_{\text{Sn}}^{(2-)}$ is strongly stabilized in Cmcm compared to Pnma.

Hall experiments by Zhao et al. [1] showed that the carrier concentration of SnSe varies strongly with T (Fig. 3). The first sign of a rapid increment in experimental electrical conductivity σ is at $T = 600$ K and continues steadily until 800 K. During the transition, the experimental concentration is well described by a single thermally activated level with energy barrier of 0.67 eV, magenta line in Fig. 3. Please note that in this small temperature interval, the $\frac{1}{T}$ behavior appears as a linear dependence on T , in Fig. 3. The magnitude of activation energy, 0.67 eV, is in good agreement with (2) the calculated Vac_{Sn}

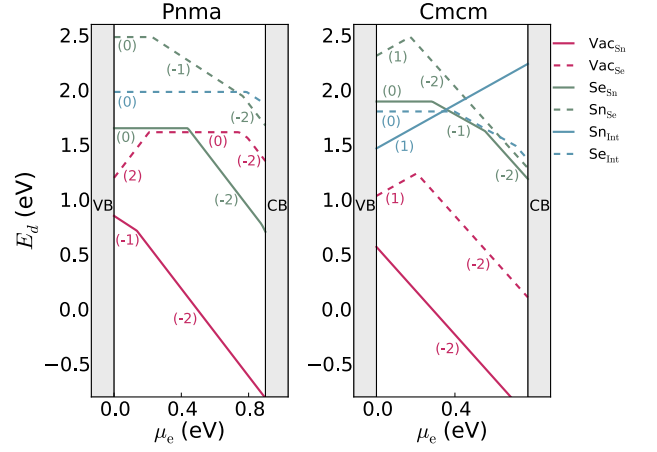


FIG. 2. The defect formation energies versus the electronic chemical potential, μ_e , are shown here for (a) the Pnma phase and for the (b) Cmcm phase in the Se rich limit. In both phases the most stable defects are the Sn vacancy, $\text{Vac}_{\text{Sn}}^{(2-)}$ (intrinsic defect) which will produce holes. The slopes of E_d versus μ_e plots are the charges of the corresponding defects.

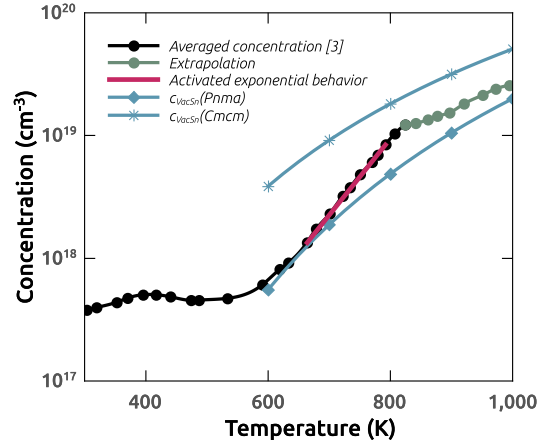


FIG. 3. Temperature dependence of the carrier concentration. In black : average inverse Hall coefficient measured by Zhao et al. [1]. In green: extrapolation determined as the carrier concentration which maximizes the Seebeck coefficient of the Cmcm phase (details in S.I.). In blue: carrier concentrations due to $\text{Vac}_{\text{Sn}}^{(2-)}$ for the Pnma and Cmcm phases. In magenta: Simple thermally activated behavior, with a defect energy of 0.67 eV.

formation energies at $\mu_e \simeq 0$ eV, Fig. 2, which strongly indicates that the increase in carrier concentration is due to creation of additional Sn vacancies during the phase transition. For temperatures below 600 K, the experimental concentration is constant for a sample that has been submitted to cycles of heating and cooling. In these conditions, the defects will be frozen into the structure with a constant carrier concentration.

Beyond a simple activated behavior, the defect formation energy will depend on temperature through μ_e ,

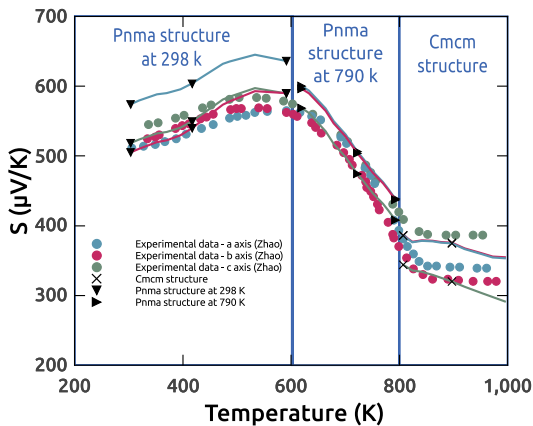


FIG. 4. Seebeck coefficients calculated with temperature-dependent carrier concentrations for three different regions of temperature. For the low-temperature region, we use the experimental structure of Pnma phase at 298 K[18]. For the intermediate region, we used Pnma experimental structure at 790 K[18]. For the last region, we used Cmcm experimental structure at 825 K[18]. These calculations are compared with Ref. [1]

Fig. 2. The temperature dependent equilibrium concentration of defects, $c_{D(q)}$, and corresponding carrier concentration, is calculated following Refs. 19 and 20, and summarized in S.I. In Fig. 3 we show the resulting calculated carrier concentrations for the Pnma and Cmcm phases alongside the experimental ones and its extrapolation for higher temperatures. Our predicted carrier concentration, essentially due to Sn vacancies, agrees with experiment above 600 K, suggesting the defects are equilibrated around this temperature. This also corresponds to the onset of the phase transition, which will affect defect mobilities. The model overestimates the carrier concentration somewhat in Cmcm, compared to our extrapolation of experiment. The slope is well reproduced, suggesting that above the phase transition the defect concentration is determined by thermodynamic equilibrium rather than being limited by mobility.

We calculate the Seebeck coefficients with the BoltzTraP code[17] which uses Density Functional Theory (DFT) electronic band structures as input parameters (details in S.I.). To take into account the temperature dependence of the carrier concentration we adjust the chemical potential such that the doping level follows the experimental concentration and its extrapolation presented in Fig. 3. To account for the phase transition, we calculate the Seebeck coefficients for three different structures. The first two are Pnma structures at 295 K and 790 K, and the third structure is Cmcm taken at 825 K. All cell parameters come from Ref. [18] and internal parameters are relaxed. The excellent agreement between experiment and theory in Fig. 4 was not present in previous publications[12, 21, 22]. We relate this level of agreement to both the variation of the carrier concentration

and a correct representation of the phase transition.

The transition path between Pnma and Cmcm is subtle: the main differences are the b/a ratio and the degree of order and bond regularity. Our theoretically relaxed Pnma lattice constants, $a = 4.2095$, $b = 4.4968$, $c = 11.7201$ Å, slightly overestimate experimental ones [1, 23] which is common in GGA-DFT. Including dispersion forces does not affect the interlayer significantly (and is counterproductive with certain functionals); we do not use them in our results below. As temperature increases, there is a continuous phase transition towards the Cmcm phase, spreading over more than 200K below the critical temperature of 807K[3]. This transition can also be induced by pressure[24]. Our theoretically relaxed Cmcm lattice parameters are $a = 4.2838$, $b = 4.2816$, $c = 6.3250$ Å, which also compare well to experimental data[1].

The harmonic phonon band structure for Pnma is dynamically stable (see S.I.) and compares well with experimental Raman and IR data at Γ [23], and theory in Ref. 25. The harmonic phonon band structure for Cmcm (see S.I.) presents a transverse optical phonon mode which is unstable at Γ along the directions to X and Y. Eigenvectors show that distortions appearing from the unstable phonon do not describe the full transition from Cmcm to Pnma: the phonon responsible for the transition must be a zone-boundary mode for the primitive cell of the Cmcm structure.

An experimental study of the phase transition[3] suggested that the transition is a 2-steps process, where firstly the atomic positions are shifted along the b axis continuously over a wide range of 200° below the transition temperature T_c and, secondly, the ratio of inter-plane cell constants changes from $b/a > 1$ to $b/a < 1$ over a range of 5 K near T_c . It is not clear that this last inversion of the cell parameters would lead to a first order structural transition. However, the recent experimental study of Zhao et al. [1] found a discontinuity at T_c in Differential Thermal Analysis (DTA), confirming there are two steps in the transition.

Inspired by these results, we create a modified Cmcm structure where $b/a > 1$ by exchanging the values of a and b . Fig. 5 (a) shows the harmonic phonon bands of this structure with two unstable modes : one at the center of the Brillouin zone and a second at the zone boundary Y point. The unstable Γ point mode is ferroelectric, identical to the unstable mode of the un-modified Cmcm structure, and does not lead to Pnma. However, the Y point instability distorts the structure as in figure 1 (b). Condensing this mode and relaxing leads to the low-temperature Pnma phase. This decomposition quantifies the 2-steps process of von Schnering: an elastic and a phononic distortion are combined to transform Cmcm to Pnma. This model explains numerous experimental results: in particular the discontinuity in the DTA originates in the elastic distortion, whereas the slow change

of transport properties, starting 200 K before T_c , comes from the gradual phononic distortion.

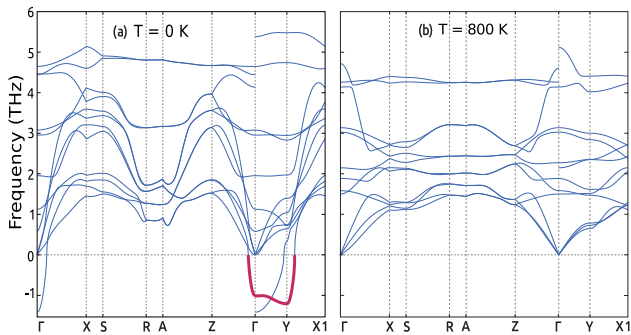


FIG. 5. Phonon band structure for SnSe in the Cmcm phase at different temperatures. (a) harmonic 0 K phonons of the modified Cmcm structure where the a and b cell parameters are exchanged. A strong harmonic instability at the Y point returns the structure to the 0 K Pnma ground state. (b) phonons of Cmcm calculated within TDEP at 807 K and for a pressure of 4 GPa - the structure is fully stabilized.

In order to verify the possibility of a metastable Cmcm phase at ambient conditions, a metadynamics calculation was performed at 0.1 GPa and two different temperatures 300 K and 700K. This is a technique to map out the local potential energy surface (PES), by adding to the Born Oppenheimer potential a repulsive term which tracks the dynamics history [15, 16, 26, 27]. Calculation details follow Ref. [28] (cf. SI).

The evolution of the metadynamics for 300K and 700K is shown in Fig. 6. The top right panel shows the Gibbs Free Energy, the bottom left the b/a ratio, and the bottom right panel the scalar product of two generalized forces on the unit cell, one coming from the PES and the other from the metadynamics Gaussians. A positive scalar product value indicates the metadynamics is moving into a well in the PES (initial phase), a negative value that it is climbing out, and a value near 0 that it is passing through saddle points between wells. The initial structure is Pnma for both temperatures. The first phase of the metadynamics is a slip of the SnSe bilayers, with rocksalt-like stacking. The dynamics then oscillates between $b/a > 1$ and $b/a < 1$. The principal conclusion is that both the layer slip and the oscillations observed do not show any metastable Cmcm phase, which validates our conclusions based on the harmonic phonons.

Our final step is to confirm the high-T stability of Cmcm. The phonon results above do not include the temperature dependence of the interatomic forces (IFCs). In order to include full anharmonicity, we use the Temperature-Dependent Effective Potential (TDEP) approach (details in S.I.)[14]. Based on ab initio molecular dynamics (MD) in the canonical ensemble, an effective potential is fit to harmonic and anharmonic IFCs. The instability of Cmcm precludes the use of finite displacement methods as in Ref. [25]. With the TDEP method

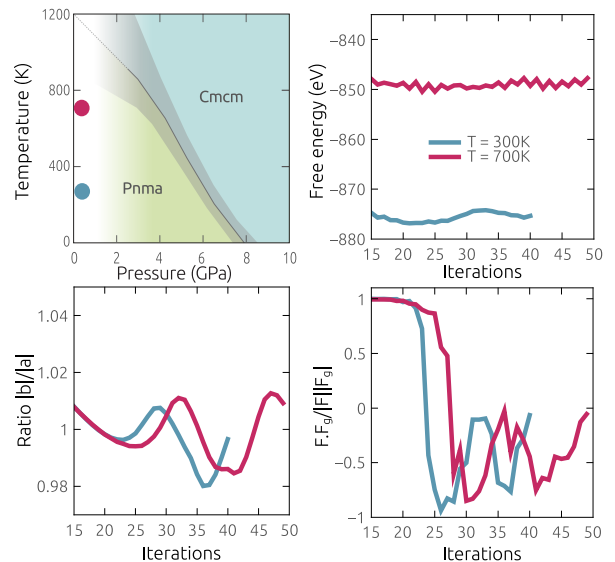


FIG. 6. Top left panel : full phase diagram of SnSe, from the TDEP method. The experimental T_c is recovered under a small volume contraction. Magenta and blue dots in the phase diagram : position in phase space for the metadynamics calculations. Top right panel : Gibbs Free energy as a function of the metadynamics step, for 0.1 GPa at 300K and 700K. Bottom left panel : b/a ratio of the crystal as function of the metadynamics step. Bottom right panel : scalar product of the metadynamics and DFT generalized forces, indicating whether one is being pushed into (> 1) or out of (< 1) a well in the PES.

the force constants come from the full potential energy surface and contain infinite order renormalization of anharmonicities at the chosen temperature. This allows us to calculate the phonon band structure at finite temperature and the anharmonic free energies[29]. The top-left panel of Fig. 6 shows the pressure-temperature phase diagram of SnSe calculated from the Gibbs free energy within TDEP. We find that the relaxed GGA volume is slightly too large, and that the phase diagram is very sensitive to it. At low pressures only Pnma structures appear in the MD: a small positive pressure is required to induce the phase transition to Cmcm. The “missing” pressure is probably linked to DFT shortcomings, such as a lack of accurate van der Waals contributions. The crystal structure is quite close to experiments, and we have tried all commonly available van der Waals functionals: none improve the results. Under a compression of around 4 GPa (volume change of 9%, faded zone in the figure), we obtain excellent agreement with experiment: the phase transition temperature of 807 K is reproduced, and the calculated phonon band structure of Cmcm is fully stabilized (Fig. 5 (b)).

In summary, we present a complete account of the origin and evolution of the huge thermoelectric properties in SnSe. The fundamental driver is the order of magnitude increase of the carrier concentration, which we show is

due to the energetics of charged defects in the two phases. Further, we decompose phonon and elastic instabilities to show that the transition from Pnma to Cmcm is indeed double, as suggested by von Schnering in 1981. There is a progressive change of bond angles over a range of 200 K, and then a first order elastic transition at around 800 K, which inverts the b/a ratio. Finite temperature phonon calculations reconstruct the full phase diagram, and are necessary to stabilize Cmcm. The strong carrier-induced electrical conductivity can thus be engineered in chalcogenides[2, 20] without destroying the thermopower as suggested by Hong *et al.*[30]. As the structures of SnSe are common in other materials classes, our analysis opens prospects for new layered and heterostructured thermoelectrics of unprecedented efficiency.

AHR acknowledges the support of NSF 1434897 and the Donors of the American Chemical Society Petroleum Research Fund under contract 54075-ND10. MJV and AD acknowledge support from ULg, two ARC grant (TheMoTherm # 10/15-03 and AIMED # 15/19-09) from the Communauté Française de Belgique, support from COST networks EUSpec (MP1306) and XLIC (CM1204), and computer time from CECI, SEGI, and PRACE-3IP (EU FP7 Grant No. RI-312763) on Archer and Lindgren. Support from the Knut & Alice Wallenberg Foundation (KAW) project “Isotopic Control for Ultimate Material Properties” and the Swedish Foundation for Strategic Research (SSF) program SRL10-002 is gratefully acknowledged. Supercomputing resources were also provided by the Swedish National Infrastructure for Computing (SNIC).

-
- [1] L.-D. Zhao, S.-H. Lo, Y. Zhang, H. Sun, G. Tan, C. Uher, C. Wolverton, V. P. Dravid, and M. G. Kanatzidis, *Nature* **508**, 373 (2014).
- [2] L.-D. Zhao, G. Tan, S. Hao, J. He, Y. Pei, H. Chi, H. Wang, S. Gong, H. Xu, V. P. Dravid, et al., *Science* **351**, 141 (2016).
- [3] H. G. von Schnering and H. Wiedemeier, *Zeitschrift für Kristallographie* **156**, 143 (1981).
- [4] J. Yang, G. Zhang, G. Yang, C. Wang, and Y. X. Wang, *Journal of Alloys and Compounds* **644**, 615 (2015).
- [5] L.-D. Zhao, G. Tan, S. Hao, J. He, Y. Pei, H. Chi, H. Wang, S. Gong, H. Xu, V. P. Dravid, et al., *Science* **351**, 141 (2016).
- [6] E. K. Chere, Q. Zhang, K. Dahal, F. Cao, J. Mao, and Z. Ren, *Journal of Materials Chemistry A* **4**, 1848 (2016).
- [7] F. Q. Wang, S. Zhang, J. Yu, and Q. Wang, *Nanoscale* **7**, 15962 (2015).
- [8] Y.-M. Han, J. Zhao, M. Zhou, X.-X. Jiang, H.-Q. Leng, and L.-F. Li, *Journal of Materials Chemistry A* **3**, 4555 (2015).
- [9] S. R. Popuri, M. Pollet, R. Decourt, F. D. Morrison, N. S. Bennett, and J. W. G. Bos, *Journal of Materials Chemistry C* (2016).
- [10] S. Rhim, J.-H. Lee, S. C. Hong, et al., *AIP Advances* **5**, 117147 (2015).
- [11] D. D. Cuong, S. H. Rhim, J.-H. Lee, and S. C. Hong, *AIP Advances* **5**, 117147 (2015).
- [12] R. Guo, X. Wang, Y. Kuang, and B. Huang, *Physical Review B* **92** (2015).
- [13] M. Verstraete and Z. Zanolli, in *Computing Solids: Models, Ab-initio Methods and Supercomputing, Lecture Notes of the 45th Spring School 2014*, edited by S. Blügel, N. Helbig, V. Meden, and D. Wortmann (Schriften des Forschungszentrums Jülich, 2014), vol. 35, p. C2.
- [14] O. Hellman, I. A. Abrikosov, and S. I. Simak, *Physical Review B* **84**, 180301 (2011).
- [15] R. Martoňák, *The European Physical Journal B* **79**, 241 (2011).
- [16] R. Martoňák, A. Laio, M. Bernasconi, C. Ceriani, P. Raiteri, F. Zipoli, and M. Parrinello, *Zeitschrift für Kristallographie* **220**, 489 (2005).
- [17] G. K. H. Madsen and D. J. Singh, *Comp. Phys. Comm.* **175**, 67 (2006).
- [18] T. Chattopadhyay, J. Pannetier, and H. V. Schnering, *Journal of Physics and Chemistry of Solids* **47**, 879 (1986), ISSN 0022-3697.
- [19] C. Bera, S. Jacob, I. Opahle, N. S. H. Gunda, R. Chmielowski, G. Dennler, and G. K. H. Madsen, *Phys. Chem. Chem. Phys.* **16**, 19894 (2014).
- [20] S. Bhattacharya, N. S. H. Gunda, R. Stern, S. Jacobs, R. Chmielowski, G. Dennler, and G. K. H. Madsen, *Phys. Chem. Chem. Phys.* **17**, 9161 (2015).
- [21] G. Shi and E. Kioupakis, *Journal of Applied Physics* **117**, 065103 (2015).
- [22] X. Guan, P. Lu, L. Wu, L. Han, G. Liu, Y. Song, and S. Wang, *Journal of Alloys and Compounds* **643**, 116 (2015).
- [23] H. Chandrasekhar, R. Humphreys, U. Zwick, and M. Cardona, *Physical Review B* **15**, 2177 (1977).
- [24] S. Alptekin, *Journal of Molecular Modeling* **17**, 2989 (2011).
- [25] J. Carrete, N. Mingo, and S. Curtarolo, *Applied Physics Letters* **105**, 101907 (2014).
- [26] A. Laio and F. L. Gervasio, *Reports on Progress in Physics* **71**, 126601 (2008).
- [27] A. Laio and M. Parrinello, in *Computer Simulations in Condensed Matter Systems: From Materials to Chemical Biology Volume 1* (Springer, 2006), pp. 315–347.
- [28] R. Martoňák, D. Donadio, A. R. Oganov, and M. Parrinello, *Nature materials* **5**, 623 (2006).
- [29] O. Hellman, P. Steneteg, I. A. Abrikosov, and S. I. Simak, *Physical Review B* **87**, 104111 (2013).
- [30] A. J. Hong, L. Li, H. X. Zhu, Z. B. Yan, J.-M. Liu, and Z. F. Ren, *Journal of Materials Chemistry A* **3**, 13365 (2015).
- [31] See supplemental material [url], which includes refs. [32–64].
- [32] X. Gonze, J.-M. Beuken, R. Caracas, F. Detraux, M. Fuchs, G.-M. Rignanese, L. Sindic, M. Verstraete, G. Zerah, F. Jollet, et al., *Computational Materials Science* **25**, 478 (2002).
- [33] X. Gonze, G.-M. Rignanese, M. Verstraete, J.-M. Beuken, Y. Pouillon, R. Caracas, F. Jollet, M. Torrent, G. Zerah, M. Mikami, et al., *Zeitschrift für Kristallographie* **220**, 558 (2005).
- [34] H. J. Monkhorst and J. D. Pack, *Physical Review B* **13**, 5188 (1976).
- [35] Y. A. Timofeev, B. V. Vinogradov, and V. B. Begoulev,

- Physics of the Solid State **39**, 207 (1997).
- [36] S. Sassi, C. Candolfi, J.-B. Vaney, V. Ohorodniichuk, P. Masschelein, A. Dauscher, and B. Lenoir, Applied Physics Letters **104**, 212105 (2014).
- [37] P. Blaha, K. Schwarz, G. Madsen, D. Kvasnicka, and J. Luitz, An Augmented Plane WaVe Plus Local Orbitals Program for Calculating Crystal Properties. ISBN 3-9501031-1-2. Vienna University of Technology: Austria (2001).
- [38] E. Engel and S. H. Vosko, Physical Review B **47**, 13164 (1993).
- [39] A. H. Romero, E. K. U. Gross, M. J. Verstraete, and O. Hellman, ArXiv e-prints (2014), 1402.5535.
- [40] O. Hellman, P. Steneteg, I. A. Abrikosov, and S. I. Simak, Physical Review B **87**, 104111 (2013).
- [41] O. Hellman and I. A. Abrikosov, Physical Review B **88**, 144301 (2013).
- [42] P. E. Blöchl, Phys. Rev. B **50**, 17953 (1994).
- [43] G. Kresse, Computational Materials Science **6**, 15 (1996).
- [44] G. Kresse, Physical Review B **59**, 1758 (1999).
- [45] G. Kresse and J. Furthmüller, Physical Review B **54**, 11169 (1996).
- [46] G. Kresse and J. Hafner, Physical Review B **48**, 13115 (1993).
- [47] J. P. Perdew, K. Burke, and M. Ernzerhof, Phys. Rev. Lett. **77**, 3865 (1996).
- [48] S. Nosé, Molecular physics **52**, 255 (1984).
- [49] W. G. Hoover, Physical Review A **31**, 1695 (1985).
- [50] P. Steneteg, O. Hellman, O. Y. Vekilova, N. Shulumba, F. Tasndi, and I. A. Abrikosov, Physical Review B **87** (2013).
- [51] M. Omini and A. Sparavigna, Physica B: Condensed Matter **212**, 101 (1995).
- [52] D. A. Broido, A. Ward, and N. Mingo, Physical Review B **72** (2005).
- [53] S. Lee, K. Esfarjani, T. Luo, J. Zhou, Z. Tian, and G. Chen, Nature Communications **5**, 3525 (2014).
- [54] R. Armiento and A. Mattsson, Physical Review B **72**, 085108 (2005).
- [55] A. Mattsson and R. Armiento, Physical Review B **79**, 155101 (2009).
- [56] R. Martoňák, A. Laio, and M. Parrinello, Physical review letters **90**, 075503 (2003).
- [57] G. I. Csonka, J. P. Perdew, A. Ruzsinszky, P. H. Philipsen, S. Lebègue, J. Paier, O. A. Vydrov, and J. G. Ángyán, Physical Review B **79**, 155107 (2009).
- [58] S. Nosé, The Journal of chemical physics **81**, 511 (1984).
- [59] S. Nosé, Progress of Theoretical Physics pp. p1–117 (1991).
- [60] D. Bylander and L. Kleinman, Physical Review B **46**, 13756 (1992).
- [61] C. G. Van de Walle and J. Neugebauer, Journal of Applied Physics **95**, 3851 (2004).
- [62] G. Makov and M. C. Payne, Physical Review B **51**, 4014 (1995).
- [63] P. B. Allen, Phys. Rev. B **17**, 3725 (1978).
- [64] G. Madsen and D. Singh, Comp. Phys. Comm. **175**, 6771 (2006).